Pergamon

SCIENCE DIRECT®

Bioorganic & Medicinal Chemistry 11 (2003) 3379–3392

BIOORGANIC & MEDICINAL CHEMISTRY

Design and Synthesis of Highly Constrained Factor Xa Inhibitors: Amidine-Substituted Bis(benzoyl)-[1,3]-diazepan-2-ones and Bis(benzylidene)-bis(*gem*-dimethyl)cycloketones

Jian Cui,[a,b] David Crich,[b] Donald Wink,[b] Matthew Lam,[c] Arnold L. Rheingold,[c] David A. Case,[d] WenTao Fu,[a] Yasheen Zhou,[a] Mohan Rao,[d] Arthur J. Olson[d] and Michael E. Johnson[a,*]

[a]*Center for Pharmaceutical Biotechnology, University of Illinois at Chicago, 900 S. Ashland Avenue, M/C 870, Chicago, IL 60607-7173, USA*

[b]*Department of Chemistry, University of Illinois at Chicago, 845 West Taylor Street, Chicago, IL 60607, USA*

[c]*Department of Chemistry, University of Delaware, Newark, DE 19716, USA*

[d]*Department of Molecular Biology, The Scripps Research Institute, La Jolla, CA 92037, USA*

Received 7 November 2002; revised 10 May 2003; accepted 13 May 2003

Abstract—Two conformationally constrained templates have been designed to provide selective inhibitors of the coagulation cascade serine protease, Factor Xa (FXa). The most active inhibitor, 2,7-bis[(*Z*)-*p*-amidinobenzylidene)]-3,3,6,6-tetramethylcycloheptanone, exhibits a K_i of 42 nM against FXa, with strong selectivity against thrombin (1000-fold), trypsin (300-fold) and plasmin (900-fold). With only two freely rotatable bonds, molecular modeling suggests that one amidine group is positioned into the S1 pocket, forming hydrogen bonds with the side chain of Asp189, similar to other amidine-based inhibitors, with the second benzamidine positioned into the S4 pocket in a position to form strong cation–pi bonding with the S4 aryl cage. We suggest that this interaction plays an important role in the specificity of these inhibitors against other serine proteases.

Introduction

Activation of the blood clotting or coagulation system is necessary to prevent blood loss after injury, but uncontrolled intravascular activation of coagulation can cause pathological thrombosis. This can lead to the serious clinical consequences of myocardial infarction, stroke, pulmonary embolism, deep-vein thrombosis and disseminated intravascular coagulation. Thromboembolic diseases are the leading causes of morbidity and mortality in most industrialized societies. Genesis of thrombosis can be induced by endothelial injury, hyperviscosity and decrease in fibrinolysis. The anatomical origin of thrombosis disorders differs according to diverse types of pathophysiology. Thrombotic disorders are a major cause of disability and death in the US, and are expected to become the leading cause of death worldwide within two decades.[1–7]

Thrombin and Factor Xa (FXa) play critical roles in thrombosis and hemostasis, with thrombin initiating clot formation, and FXa providing the sole mechanism for thrombin activation. Thrombin and related proteases involved in blood coagulation have been studied extensively over many years. Although heparin and the coumarin anticoagulants are long-established treatments in coagulation disorders, side effects, limitations of efficacy and bleeding complications with these agents have stimulated intense searches for more direct and specific inhibitors of key enzymes in the coagulation cascade.[1–4,6]

There is substantial evidence suggesting that FXa should be an attractive target for inhibitor design. Several organisms have developed specific peptidic inhibitors that selectively target FXa, and provide very potent

*Corresponding author. Tel.: +1-312-996-9114; fax: +1-312-413-9303; e-mail: mjohnson@uic.edu

0968-0896/03/$ - see front matter © 2003 Elsevier Ltd. All rights reserved.
doi:10.1016/S0968-0896(03)00332-8

anticoagulant activity. For example, tick anticoagulant peptide exhibits very selective inhibition of FXa with a K_i of 180 pM, and, in a variety of animal models, has been shown to be equal to, and in many cases, superior to traditional heparin therapy or recombinant hirudin as an antithrombotic agent.[8] Similarly, the leech protein antistasin exhibits selective inhibition of FXa, and has been shown to be substantially more effective than heparin in models of arterial thrombosis and in reocclusion prophylaxis.[6,9,10] A series of anticoagulant peptides produced by the hookworm *Ancylostoma caninum* also exhibit selective inhibition of both FXa and Factor VIIa.[11] Additionally, several comparisons between direct thrombin inhibitors and direct FXa inhibitors in animal models have shown inhibitors of FXa to be superior antithrombotic agents[12–14] with lower bleeding risk–antithrombotic benefit ratios.[15,16]

A number of FXa inhibitor designs have been described recently, with most based on moderately flexible linkers connecting various substituents that exhibit affinity for the FXa S1 and S4 subsites.[1–5,7,17,18] Docking studies have suggested that binding in an L-shaped configuration, with a 'recognition' moiety inserted into the S1 specificity pocket, and an aromatic or aryl cationic group inserted into the aromatic cage formed by Tyr99, Phe174 and Trp215 is especially favored.[19] The BABCH inhibitors, shown in Figure 1, are particularly intriguing probes of specificity between FXa and related serine proteases.[20,21] With essentially only two degrees of freedom within the molecule (rotation of the benzamidine groups), the most active structure (the *Z*,*Z* or *syn* isomer shown here) exhibits very high FXa inhibitory activity, with a $K_i \sim 0.66$ nm, and an approximate 800-fold difference in inhibitory activity between FXa and thrombin.[20,21] The initial description of these inhibitors suggested that they were in the extended *E*,*E* configuration.[22] More recent work, however, has shown that there is photo conversion between the *E*,*E*, *E*,*Z* and *Z*,*Z* isomers in the presence of light, and that the *Z*,*Z* isomer is 25,000 times more active than the *E*,*E* isomer, but is present at only trace levels at equilibrium in the presence of light.[20,21]

In the present work, we have devised two alternative, conformationally constrained structural templates that stabilize the *Z*,*Z* or *syn* configuration, and have developed an initial lead that has an FXa dissociation constant of ~42 nM, and 250–1000-fold selectivity against trypsin, plasmin and thrombin.

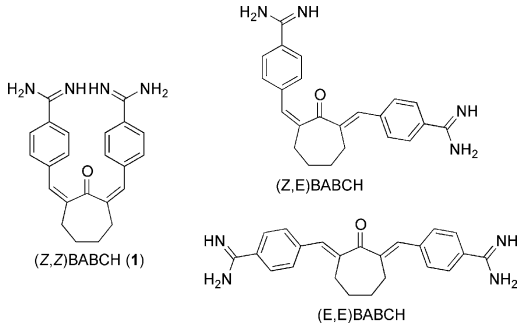

Figure 1. BABCH isomers.

Inhibitor Design

Owing to the two double bonds adjoining the central ring, BABCH has three possible isomers (*Z*,*Z*), (*E*,*Z*) and (*E*,*E*) (Fig. 1). As a first step in developing alternative templates, we developed a detailed conformational analysis of BABCH. To obtain computationally reliable results, we found it necessary to utilize Gaussian ab initio calculations. Our Gaussian calculations, performed at the HF/3-21G level to provide reliable energies and geometries, indicate that the extended (*E*,*E*) isomer has a conformational energy about 2 kcal/mol lower than the V-like (*Z*,*Z*) isomer, which is consistent with the conformational population distribution that can be inferred from the observed K_i values.[20,21] The lowest energy conformers of all three isomers have the same central ring conformation, a pseudo-chair conformation. The relative positioning of the benzamidine rings in the calculated (*Z*,*Z*)BABCH conformation is also very close to that experimentally observed in the BABCH/tissue-type plasminogen activator (tPA) complex.[23]

The observed binding mode of BABCH with tPA[23] differs from that initially predicted for the (*Z*,*Z*)BABCH-FXa complex.[20] Accordingly, to determine the most probable binding mode, we docked a molecular model of the calculated (*Z*,*Z*)BABCH into the active site of the FXa crystal structure[24] with the Autodock program,[25,26] using the calculated (*Z*,*Z*)BABCH conformation, and allowing free rotation only for the benzamidine groups and limited rotation of $\pm 25°$ for the amidine groups. We find that the most probable binding mode positions one benzamidine group into the S1 pocket, and the second into the S4 pocket, as shown in Figure 2. In this model, the benzamidine in the S1 specificity pocket exhibits bidentate hydrogen bonding with the Asp189 carboxylate. The heptanone ring carbonyl is positioned to permit hydrogen bonding to the Gly216 amide, shifted somewhat further away from the Tyr99 wall of the S4 site than observed for the BABCH–tPA complex.[23] The distal benzamidine is inserted at a slight angle into the S4 pocket, with the amidine slightly

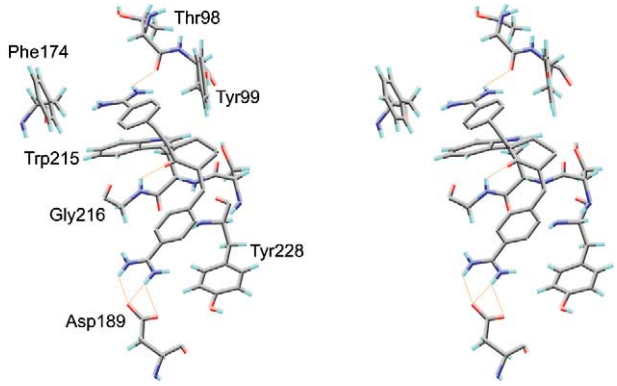

Figure 2. Relaxed stereo view of the computational model of (*Z*,*Z*)BABCH (**1**) docked into the active site of Factor Xa. The BABCH model conformation was determined by Gaussian calculations. In docking, the benzamidine groups were allowed to rotate freely and the amidines were allowed $\pm 25°$ rotation with respect to the plane of the phenyl ring.

pointed up toward the carbonyl cluster,[27] forming a hydrogen bond with the carbonyl of Thr98, and nearly centered in the aryl cage formed by the Tyr99 phenole, the Trp215 indole and the Phe174 phenyl rings. Overall, the modeled binding mode of BABCH with FXa is similar to that experimentally observed for the BABCH–tPA complex,[23] despite the differences in the S4 subsite between the two enzymes. The distal amidine also appears to be almost ideally positioned within the S4 aryl cage to provide additional cation–pi stabilization for this binding mode that should be unique to Fxa.[28] Based on this analysis, an alternative template that can stabilize the (*Z*,*Z*)BABCH configuration should provide an effective FXa inhibitor with good enzymatic specificity.

To take advantage of the *Z*,*Z*-BABCH structure, but at the same time avoid its stability problems, we focused on modifying the central skeleton. Two potential isosteric scaffolds were designed to render the symmetrical cycloheptadienone core of (*Z*,*Z*)BABCH into a less photochemically sensitive and more synthetically feasible pharmacophore (Fig. 3). The first template is a seven-membered cyclic urea in which two amide bonds were chosen to replace the problematic double bonds. The new amide bonds have the advantages of keeping the original double bond characteristics, thereby maintaining a similar geometry, and avoiding the isomer problem. The energy difference between the *syn* and *anti* configuration is calculated to be about 8.4 kcal/mol, favoring the folded *syn* configuration (Fig. 4). The second template is a bis-*gem*-tetramethylcycloheptanone. In this system,[1,3] A-strain between the four methyl groups and the phenyl rings should destabilize the (*E*,*E*) isomer and so favor a *syn*-conformation similar to the (*Z*,*Z*)BABCH. The energy difference between the (*Z*,*Z*) and the (*E*,*E*) isomers is calculated to be about 2.8 kcal/mol, favoring a *syn*-conformation similar to that of (*Z*,*Z*)BABCH. We therefore predicted that the designed templates should maintain the same geometry as (*Z*,*Z*)BABCH, with a substantially decreased possibility of isomerization. Based on this analysis, the synthesis of both templates I and II was undertaken with several variations.

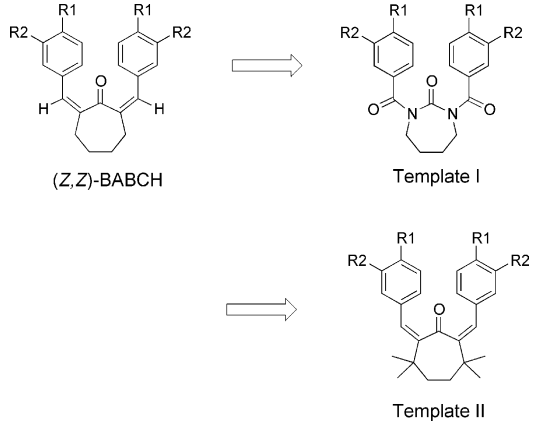

Figure 3. Alternate templates for the central heptanone ring of BABCH expected to stabilize the folded *syn* configuration.

Chemistry

Template I

The synthesis of 1,3-bis(3-amidinobenzoyl)-[1,3]-diazapan-2-one (**2**) is shown in Scheme 1. Deprotonation of the bis-amide (**3**) with a single equivalent of lithium hexamethyldisilazide (LiHMDS), followed by treatment with 4-nitrophenyl chloroformate and then a second equivalent of LiHMDS furnished the *N*,*N*′-diacyl urea (**4**) in 45% overall yield. This was most effectively converted to the bis amidine (**2**) via the symmetrical thioamide (**5**) and the bis-thioimidate (**6**) by treatment with

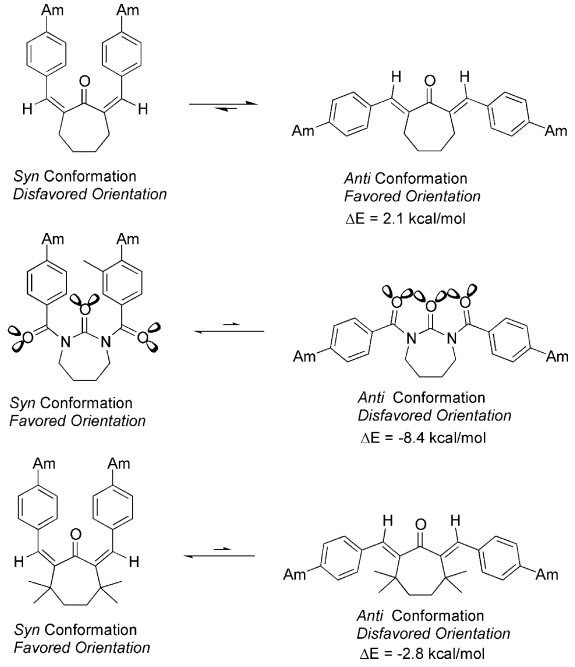

Figure 4. Comparative energies for the folded (*syn*) conformations relative to the extended (*anti*) conformations for (*Z*,*Z*)BABCH and templates I and II, as calculated by Gaussian (HF/3,21).

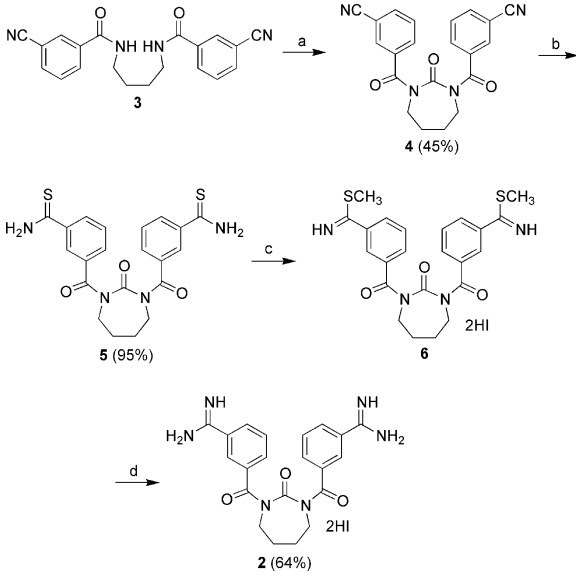

Scheme 1. (a) 1 equiv LiHMDS, THF, −78 °C; *p*-$NO_2C_6H_4OC(=O)Cl$; 1 equiv LiHMDS, −78 °C to rt; (b) $(EtO)_2P(=S)SH$, rt; (c) MeI, Δ; (d) NH_3–HOAc, 0 °C (two steps).

diethyl dithiophosphate,[29–31] methyl iodide, and ammonium acetate. The attempted conversion of the bis-nitrile **4** to the bis-amidine **2** by the more usual Pinner reaction,[32–34] involving sequential treatment with Hal in methanol and then ammonia, served only to illustrate the relative susceptibility of the system toward nucleophilic attack on the tricarbonyl system, and was a harbinger of the problems subsequently encountered in the corresponding *p*-substituted series.

All attempts at application of the same sequence to preparation of the corresponding 1,3-bis(4-amidinobenzoyl)-[1,3]-diazapan-2-one (**7**) failed at the last step (Scheme 2), apparently because of the enhanced electrophilicity of the diacyl urea system resulting from conjugation of the powerfully electron-withdrawing amidinium groups. An alternative synthesis involving hydrogenolysis of the less basic, stable *N*,*N*′-diacetoxy bisamidine (**13**), derived by reaction of the bisthioimidate **11** with hydroxylamine followed by acetylation, also failed to provide **7**.

Template II

It was envisaged that the target compound, 2,7-bis[(*Z*)-*p*-amidinobenzylidene)]-3,3,6,6-tetramethylcycloheptanone, could be synthesized by double aldol condensation of two equivalents of 4-cyanobenzaldehyde with 3,3,6,6-tetramethylcycloheptanone. The literature approaches[35,36] to 3,3,6,6-tetramethylheptanone (**15**) were deemed inappropriate for our purposes, and a route (Scheme 3) was developed in which 4,4-dimethylcyclohexanone was converted to 3,3,6-trimethylcycloheptenone (**14**), according to a literature protocol,[37,38] followed by conjugate addition in the standard manner.

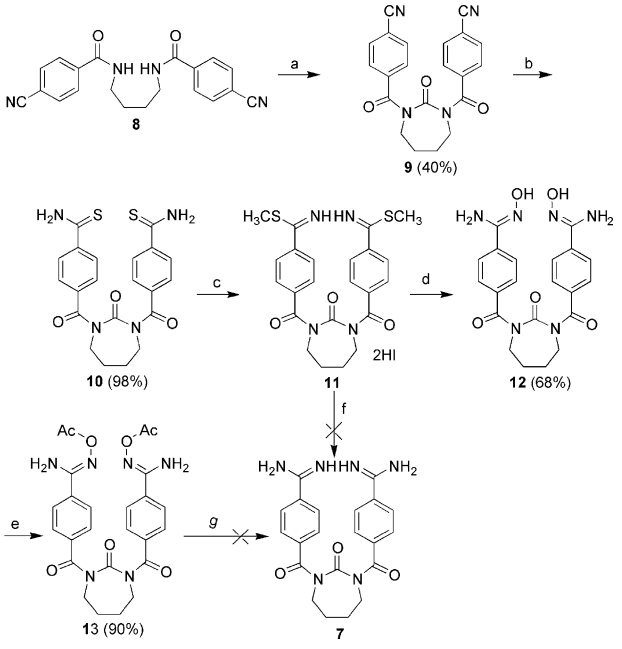

Scheme 2. (a) 1 equiv LiHMDS, THF, −78 °C; *p*-$NO_2C_6H_4OC(=O)Cl$; 1 equiv LiHMDS, THF, −78 °C to rt; (b) $(EtO)_2P(=S)SH$, rt; (c) MeI, Δ; (d) NH_2OH–HCl, Et_3N, 0 °C; (e) CH_3COCl, Et_3N, 0 °C; (g) Pd/C, H_2; (g) NH_3–HOAc, 0 °C.

At the same time, the commodity substance isophorone was converted to the lower homologue 3,3,5,5-tetramethylcyclohexanone (**17**), also by conjugate methylation, in order to provide a second analogue for testing and a more readily available substance with which to develop the double aldol chemistry.

Thus, 2,6-bis[(*Z*)-*p*-cyanobenzylidene]-3,3,5,5-tetramethylcyclohexanone (**16**) was prepared through a modified Mukaiyama reaction as shown in Scheme 4. The TMS enol ether **18** was reacted with acetal **19** and titanium tetrachloride in refluxing dichloromethane to give **20** in 67% yield along with 10% of the dicoupled product **16**. Iteration of the Mukaiyama reaction sequence on the isolated mono-coupled product **20** provided first the silyl enol ether **21** and then the desired doubly acylated product **16** in yields of 95 and 62%, respectively. Analogues, 2-[(*Z*)-*m*-cyanobenzylidene]-6-[(*Z*)-*p*-cyanobenzylidene]-3,3,5,5-tetramethylcyclohexanone (**22**) and 2,6-bis[(*Z*)-*m*-cyanobenzylidene]-3,3,5,5-tetramethylcyclohexanone (**23**), were synthesized following the same procedure. NOESY spectra were obtained and the (*Z*,*Z*)-configurations were confirmed for all. However, after exposure to ambient light for several days, olefin isomerization occurred, and **20** was converted into a mixture of *E* and *Z* isomers. Similarly, light stimulated the isomerization of **16** into a mixture of (*Z*,*Z*) and (*Z*,*E*) isomers. This may due to the relatively low energy difference (∼1 kcal/mol) between the *Z*- and *E*-configurations of these particular cyclohexanone compounds.

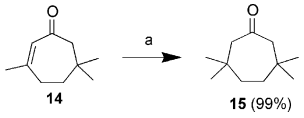

Scheme 3. (a) CuBr–Me_2S, MeLi.

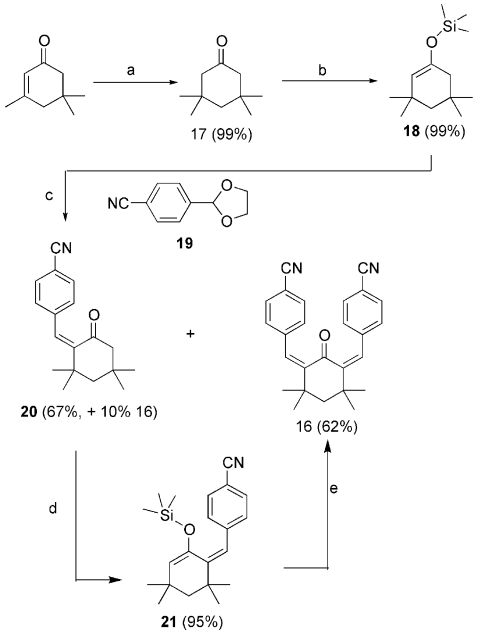

Scheme 4. (a) CuBr–Me_2S, MeLi/Et_2O; (b) TMSCl, Et_3N, NaI; (c) $TiCl_4/CH_2Cl_2$; (d) TMSCl, Et_3N, NaI; (e) $TiCl_4/CH_2Cl_2$, **19**, Δ.

In the tetramethylcycloheptanone series, the aldol condensation was significantly more difficult and it was found necessary to use the higher boiling point solvent 1,2-dichloroethane (bp 85 °C) to increase the reaction temperature. After heating **24** with three equivalents of **25**, a more reactive acetal of *p*-cyanobenzaldehyde, and two equivalents of titanium tetrachloride in refluxing 1,2-dichloroethane overnight, a mixture of mono-coupling product **26** and di-coupling product **28** were obtained in yields of 41 and 5%, respectively. After a further Mukaiyama reaction on **26**, 2,7-bis[(*Z*)-*p*-cyanobenzylidene] - 3,3,6,6 - tetramethylcycloheptanone (**28**) was finally obtained in 43% yield from **26** (Scheme 5). Analogues, 2-[(*Z*)-*m*-cyanobenzylidene]-7-[(*Z*)-*p*-cyanobenzylidene] - 3,3,6,6 - tetramethylcycloheptanone (**29**) and 2,7-bis[(*Z*)-*m*-cyanobenzylidene]-3,3,6,6-tetramethylcycloheptanone (**30**), were synthesized following the same procedure. NOESY spectra were again obtained and (*Z*,*Z*)-configurations were confirmed for all compounds. Compared to the cyclohexanones **20** and **16**, **26** and **28** are photochemically stable, and no significant isomerization occurred after exposure to light. This obviously reflects the more significant energy difference between the *E*- and *Z*-configurations, as determined computationally, between the cycloheptanone and cyclohexanone series. The more hindered nature of the cycloheptanone is also reflected in the considerably more forcing aldol conditions required.

Finally, the complete series of nitriles was converted to the corresponding amidines by Pinner's method (Scheme 6). The final products were isolated by HPLC. NOESY spectra were obtained and (*Z*,*Z*)-configurations were confirmed for all (Tables 1 and 2; additional data in Supporting Information).

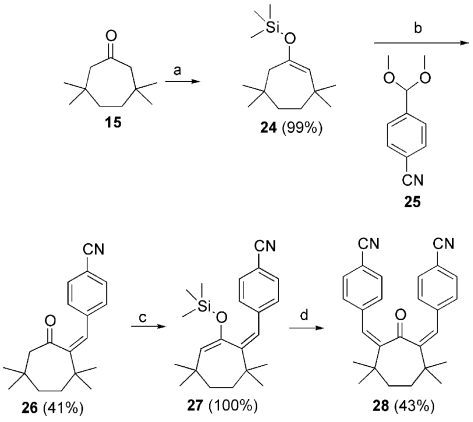

Scheme 5. (a) TMSCl, Et_3N, NaI; (b) $TiCl_4$, Δ, $ClCH_2CH_2Cl$; (c) TMSCl, Et_3N, NaI; (d) **25**, $TiCl_4$, Δ, $ClCH_2CH_2Cl$.

Results and Discussion

The crystal structure of the cyclic urea template cyano intermediate **9** is shown in Figure 5, from which it can be

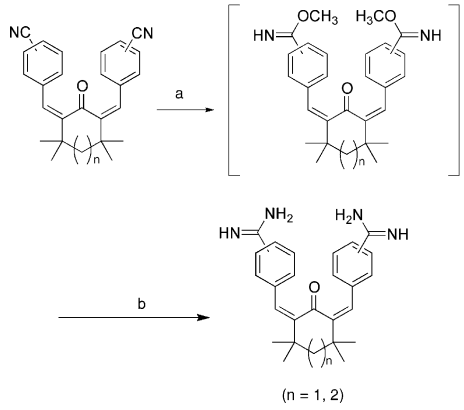

Scheme 6. (a) HCl(g), CH_3OH; (b) NH_4OAc, CH_3OH.

Table 1. ^1H and NOESY data for bisamidine compounds **31**–**33**

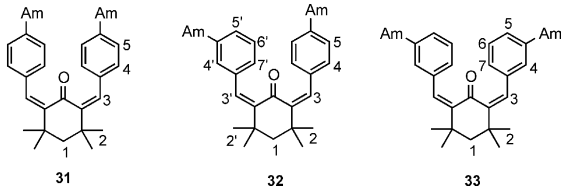

Proton	31		32		33	
	^1H	NOESY	^1H	NOESY	^1H	NOESY
1	1.90 (s)	H2	1.87 (s)	H2,2′	1.86 (s)	H2
2	1.39 (s)	H1,3	1.37 (s)	H1,3	1.38 (s)	H1,3
3	6.86 (s)	H2,4	6.84 (s)	H2,4	6.83 (s)	H4,7
4	7.43 (d)	H3	7.70–7.30 (m)	H3	7.71–7.26 (m)	H3
5	7.63 (d)		7.70–7.30 (m)		7.71–7.26 (m)	
6					7.71–7.26 (m)	
7					7.71–7.26 (m)	H3
2′			1.37 (s)	H1,3′		
3′			6.84 (s)	H2′,4′,7′		
4′			7.70–7.30 (m)	H3′		
5′			7.70–7.30 (m)			
6′			7.70–7.30 (m)			
7′			7.70–7.30 (m)	H3′		

Table 2. ^1H and NOESY data for bisamidine compounds **34**–**36**

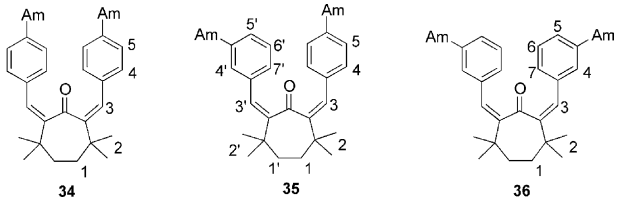

Proton	34		35		36	
	^1H	NOESY	^1H	NOESY	^1H	NOESY
1	1.81 (s)	H2	1.82 (s)	H2	1.81 (s)	H2
2	1.29 (s)	H1,3	1.30 (s)	H1,3	1.30 (s)	H1,3
3	6.71 (s)	H2,4	6.73 (s)	H2,4	6.72 (s)	H4,7
4	7.30 (d)	H3	7.88–7.25 (m)	H3	7.67–7.21 (m)	H3
5	7.52 (d)		7.88–7.25 (m)		7.67–7.21 (m)	
6					7.67–7.21 (m)	
7					7.67–7.21 (m)	H3
1′			1.82 (s)	H2′		
2′			1.29 (s)	H1,3′		
3′			6.72 (s)	H2′,4′,7′		
4′			7.88–7.25 (m)	H3′		
5′			7.88–7.25 (m)			
6′			7.88–7.25 (m)			
7′			7.88–7.25 (m)	H3′		

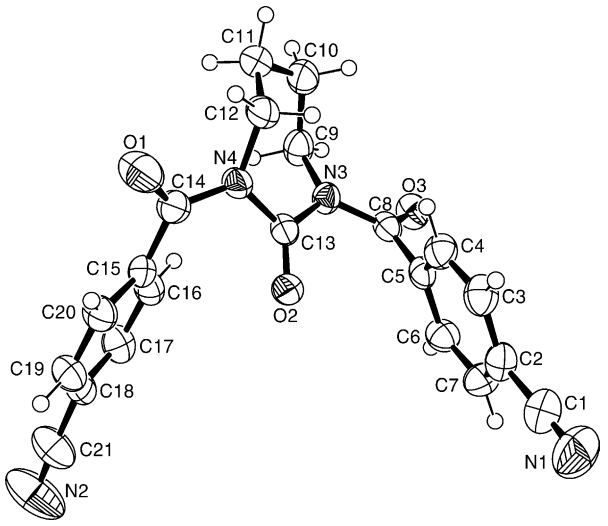

Figure 5. ORTEP plot for the crystal structure of **9**.

seen that the predicted twist structure for the central ring is observed, with the two 'arms' in the folded *syn* configuration, analogous to the Z,Z configuration of BABCH, also as predicted, positioning the two phenyl rings with a separation almost identical to that of the separation observed for BABCH crystallized with tPA,[23] indicating that the cyclic urea template is an excellent mimic for the central heptanone ring of BABCH.

FXa, thrombin, trypsin and plasmin K_i's were obtained from in vitro enzyme affinity assays at 37 °C (Table 3). Bisthioamides **5** and **10** were tested together with 3,3′-bisamidine **2**. Surprisingly, the 4,4′-bisthioamide **10** showed a FXa K_i of 0.82 μM, which is relatively potent considering there are no positive charges on it and the thioamide could only form weak hydrogen bonds. 3,3′-Bisamidine **2** showed FXa K_i at 150 nM. All three compounds were selective toward FXa over thrombin, trypsin and plasmin.

All six gem-dimethyl amidine analogues were tested to obtain their FXa, thrombin, trypsin and plasmin K_i's from in vitro enzyme affinity assays at 37 °C (Table 4). K_m and ν_{max} values were also obtained under the same conditions from the Michaelis–Menten equation.[39] K_i values were calculated using Dixon analysis.[40] Among the various analogues, 2,7-bis[(*Z*)-*p*-amidinobenzylidene)]-3,3,6,6-tetramethylcycloheptanone (**34**) is the most active, with an FXa K_i of 42 nM. It also shows high selectivity over thrombin (1000-fold), trypsin (300-fold) and plasmin (900-fold).

The other bis(*gem*-dimethyl)cycloketone compounds with amidino groups in the *meta*-positions or mixed *meta*-, *para*-positions showed neither good activity nor selectivity. They are all in the same activity range as (*E*,*E*)BABCH (FXa $K_i = 17$ μM) and showed different inhibitory characteristics than the 4,4′-bisamidines, **34** and **31**. Modeling suggests that a 3-benzamidine in the proximal position has only one NH_2 group that can hydrogen bond to the Asp189 carboxylic acid, losing the bidentate hydrogen bonding characteristic of most amidine-based inhibitors. A 3-benzamidine in the distal position also enters the S4 subsite at an unfavorable angle, generating a bumping collision with the Tyr99 side chain that forces the amidine up away from the Trp215 indole ring. These unfavorable interactions at both the S1 and S4 subsites are a probable source for the sharply reduced activities of analogues containing amidines in the 3-position.

Table 3. In vitro inhibitory activities of cyclic ureas

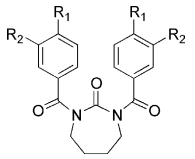

			K_i (μM)			
Compd	R_1	R_2	Factor Xa	Thrombin	Trypsin	Plasmin
5	H		13.9	110	260	>500
10		H	0.82	15.2	120	>500
2	H		0.15	8.8	1.7	24

In order to experimentally check the geometry of the designed template, the structure of one of the synthetic intermediates, 2,7-bis[(*Z*)-*p*-cyanobenzylidene]-3,3,6,6-tetramethylcycloheptanone (**28**), was determined by X-ray crystallography (Fig. 6). As expected, the four methyl groups at the β positions were able to force the two phenyl rings up and maintain the olefin double bonds in the (*Z*,*Z*) configuration. Thus, the crystal structure is in very good agreement with the computationally derived structure and is confirmed to be in the same geometry as (*Z*,*Z*)BABCH.

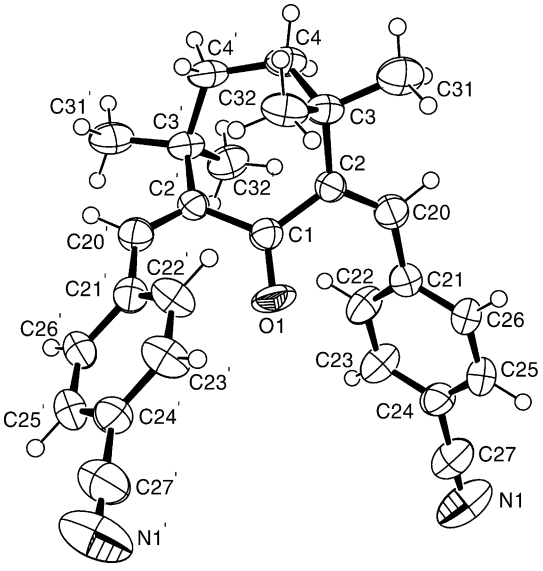

Figure 6. ORTEP plot for the crystal structure of **28**.

Table 4. In vitro inhibitory activities of the amidine-substituted (bis)benzylidene-(bis)*gem*-tetramethylcycloketones

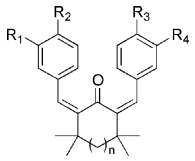

K_i (μM)									
Compd	*n*	R^1	R^2	R^3	R^4	Factor Xa	Thrombin	Trypsin	Plasmin
31	1	H			H	0.13	8.3	3.1	38
32	1		H		H	3.7	12	32	290
33	1		H	H		5.3	55	9.5	>500
34	2	H			H	0.042	42	11	25
35	2		H		H	3.2	7.9	2.3	55
36	2		H	H		6.5	11	11	>500

The inhibitory activity of **34**, the *gem*-dimethyl analogue of (*Z*,*Z*)BABCH is quite promising, but is substantially lower than that of (*Z*,*Z*)BABCH itself. To better understand the interactions of the various analogues with FXa, computational models based on the crystal structures of the intermediates for both templates (Figs 5 and 6) were docked with FXa. For the cyclic urea template (I), the amidine group within the S1 site for the cyclic urea model (Fig. 7) also forms bidentate hydrogen bonds with Asp189. The central carbonyl of the cyclic urea ring is positioned similar to that of the (*Z*,*Z*)BABCH model, permitting hydrogen bonding to the Gly216 amide. The distal benzamidine group is inserted into the S4 aryl cage in a fashion similar to that observed for the BABCH–tPA complex,[23] with the benzamidine ring nearly perpendicular to the indole ring of Trp215, and one side of the amidine positioned to form a hydrogen bond with the carbonyl of Thr98. With pharmacophores other than the benzamidines used here, this template shows promise for other inhibitor designs.

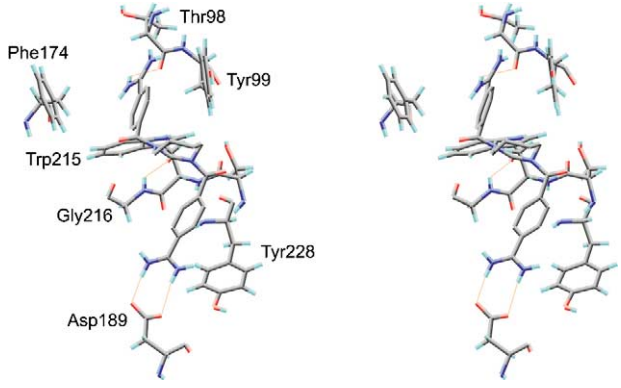

Figure 7. Relaxed stereo view of a model of **7** docked into the active site of Factor Xa using Autodock. The model of **7** was constructed by substituting amidines for the cyano groups in the intermediate crystal structure **9** (Fig. 5). The benzamidine groups were allowed to rotate freely, and the amidines allowed ±25° rotation with respect to the plane of the phenyl ring. All other angles were maintained at the values found in the crystal structure.

For the *gem*-dimethyl heptanone template (II), the benzamidine group is rotated within the S1 subsite to form a bridged hydrogen bond between one side of the amidine and the two Asp189 carboxyl oxygens, in contrast to the bidentate positioning of *Z*,*Z*-BABCH (Fig. 8). The other side of the amidine forms a hydrogen bond with the hydroxyl oxygen of Tyr228. The heptanone ring is consequently rotated away from the backbone chain, with the carbonyl roughly perpendicular to the peptide backbone, but close to the amide of Trp215. The distal benzamidine is inserted into the S4 aryl cage in an orientation similar to that of the (*Z*,*Z*)BABCH model, although tilted up somewhat more with respect to the plane of the Trp215 indole ring, and not within hydrogen bonding proximity of the Thr98 carbonyl. The interaction between the Tyr99 ring and the axial methyl of this inhibitor pushes the heptanone ring back from the S4 pocket, and appears to produce a less optimal binding mode, which may be the source of the reduced inhibitory activity, as compared to (*Z*,*Z*)BABCH. The distal benzamidine is positioned

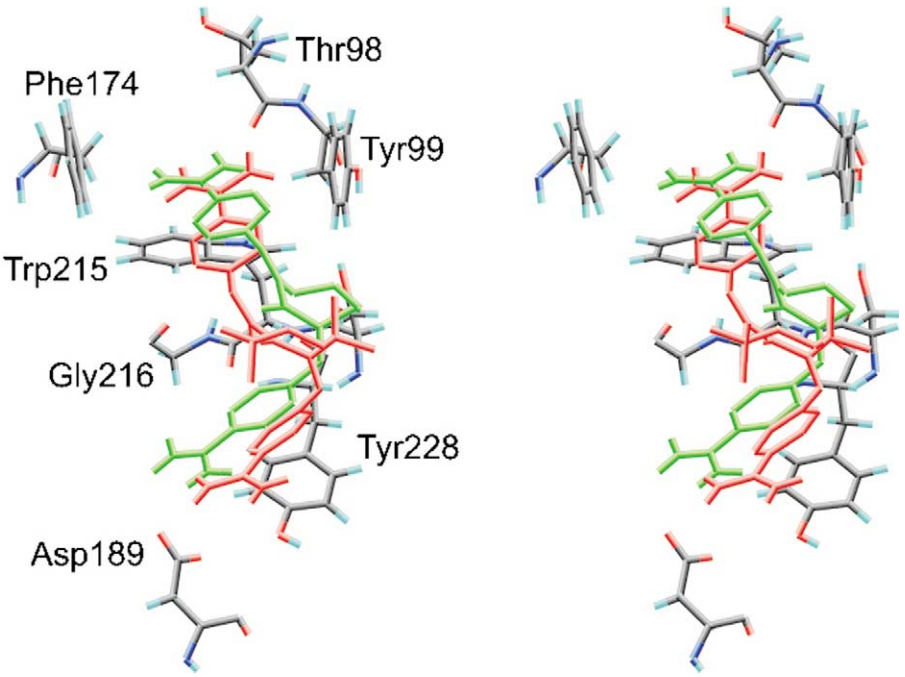

Figure 8. Relaxed stereo view of a superposition model of **34** (red) and (*Z*,*Z*)-BABCH (green) docked into the active site of factor Xa using Autodock. The model of **34** was constructed by substituting amidines for the cyano groups in the intermediate crystal structure **28** (Fig. 6). The benzamidine groups were allowed to rotate freely; the amidines were allowed ±25° rotation with respect to the plane of the phenyl ring. All other angles were maintained at the values found in the crystal structure.

within the S4 aryl cage in a manner nearly ideal for maximizing cation–pi interactions.[28] Comparative Gaussian calculations for a benzamidine centered in an aryl cage versus a similar cage with aliphatic side chains replacing the Phe and Tyr rings show a difference of about 3 kcal/mol in favor of the aryl cage, and suggest that cation–pi stabilization of the amidine within the aryl cage is the most probable source for the observed enzymatic specificity (Table 4).

Conclusions

The cyclic urea template is structurally quite attractive, but the central ring lacks the stability necessary for benzamidine substituents with *p*-amidines. It may, however, be a useful template for less basic groups that have been used in a variety of other designs. This will be explored in future work.

With only two freely rotatable bonds, the most active structure, **34**, has an FXa K_i of 42 nM. It also shows strong selectivity against thrombin (1000-fold), trypsin (300-fold) and plasmin (900-fold). Modeling indicates that it should bind in a mode qualitatively similar to that of (*Z*,*Z*)BABCH, with cation–pi interactions providing enzymatic selectivity, but with subtle differences in positioning within both the S1 and S4 subsites. A bumping collision between the Tyr99 phenolic ring and the adjacent methyl of the gem-dimethyl analogue is the most probable source for the difference in activity between **34** and (*Z*,*Z*)-BABCH. The high selectivities against thrombin and plasmin are particularly encouraging, indicating that we have, in fact, achieved our goal of selective inhibition of FXa. The activity trends, in relation to structure, are also intriguing. There is only modest variation in activity for all of these structures with thrombin, trypsin and plasmin, suggesting that there is specificity pocket (Asp189) recognition of the benzamidine group, but only modest affinity for other moieties of the inhibitor, consistent with our design goals. For FXa, however, there is a clear preference for placing both amidines in the 4-position, for both the six- and seven-member central rings. Likewise, just as for the parent (*Z*,*Z*)BABCH, there is a significant increase in activity in going from the six-member cyclohexane analogue to the seven-member cycloheptane analogue. (Going to larger ring sizes is not likely to be useful, as larger ring systems for the parent BABCH structure exhibit significantly reduced activity.) These results provide a strong foundation for further work with this series of conformationally highly constrained inhibitors.

Experimental

General

All solvents were dried and distilled by standard methods. All reactions were carried out in dried solvents under an atmosphere of argon. ^{1}H NMR spectra were acquired at either 300 or 400 MHz and ^{13}C NMR spectra at 75.5 MHz. Chemical ionization (CI) and electrospray (ESI) mass spectra were recorded on a Finnigan MAT 90 or LCQ mass spectrometer, respectively. FABHRMS were recorded with a VG 7070-HF mass spectrometer at the University of Minnesota mass spectrometry laboratory. Melting points are uncorrected. Elemental analyses were performed by Midwest Microlab (Indianapolis, IN, USA).

***N,N′*-Bis(4-cyanobenzoyl)-1,4-diaminobutane (8).** A suspension of 4-cyano-benzoic acid (25.0 g, 0.17 mol) in thionyl chloride was heated to reflux until it became clear. Thionyl chloride was distilled off under reduced pressure. The residue was dissolved in anhydrous DMF (100 mL). The resulting solution was cooled to 0 °C and triethylamine (30.0 mL, 0.19 mol) was added slowly. Then 1,4-diaminobutane (8.5 mL, 0.085 mol) was added dropwise via syringe. The reaction mixture was warmed up to room temperature and stirred overnight. The reaction mixture was poured into ice-cold 10% HCl solution. The resulting precipitate was filtered and washed twice with ice cold 10% NaOH solution and then several times with water. The solid was dried at 50 °C under vacuum to give *N,N′*-bis(4-cyanobenzoyl)-1,4-diaminobutane (26.4 g, 90%) as a slightly yellow powder (mp 264–265 °C). ^{1}H NMR (300 MHz, DMSO-d_6) δ 8.72 (2H, t, J = 5.4 Hz), 7.99 (4H, d, J = 8.7 Hz), 7.95 (4H, d, J = 8.7 Hz), 3.31 (4H, m), 1.58 (4H, m); APT ^{13}C NMR (75.5 MHz, DMSO-d_6) δ 165.6 (up), 139.4 (up), 133.3 (down), 128.9 (down), 119.2 (up), 114.3 (up), 39.9 (up), 27.3 (up); CI–MS *m/e* 347 $(M+1)^+$. Anal. calcd for $C_{20}H_{18}N_4O_2 \cdot 0.2H_2O$ C, 68.64; H, 5.30; N, 16.01. Found: C, 68.56; H, 5.43; N, 16.01.

***N,N′*-Bis(3-cyanobenzoyl)-1,4-diaminobutane (3).** **3** was prepared by the same method described above for the synthesis of **8** using 3-cyanobenzoic acid as starting material (90% from 3-cyanobenzoic acid, mp 203–204 °C). ^{1}H NMR (300 MHz, DMSO-d_6) δ 8.70 (2H, t, J = 5.6 Hz), 8.25 (2H, s), 8.14 (2H, d, J = 7.8 Hz), 7.99 (2H, d, J = 7.8 Hz), 7.68 (2H, t, J = 7.8 Hz), 3.32 (4H, bs), 1.58 (4H, bs); APT ^{13}C NMR (75.5 MHz, DMSO-d_6) δ 165.1 (up), 136.4 (up), 135.4 (down), 132.9 (down), 131.6 (down), 130.6 (down), 119.2 (up), 112.5 (up), 39.9 (up), 27.3 (up); CI–MS *m/e* 347 $(M+1)^+$. Anal. calcd for $C_{20}H_{18}N_4O_2$ 1/4H_2O: C, 68.46; H, 5.31; N, 15.97. Found: C, 68.51; H, 5.31; N, 15.82.

1,3-Bis(4-cyanobenzoyl)-[1,3]-diazepan-2-one (9). Under a nitrogen atmosphere, a solution of LiHMDS in THF (1.0 M, 6.3 mL) was added dropwise to a suspension of **8** (2.0 g, 5.8 mmol) in 250 mL THF at −78 °C. The reaction mixture was stirred for 30 min, and 4-nitrophenyl chloroformate (1.3 g, 6.3 mmol) was added in. The mixture was warmed up to room temperature and stirred for another 30 min. Then the reaction mixture was cooled to −78 °C again and a solution of LiHMDS in THF (1.0 M, 6.3 mL) was added in dropwise. After stirring at room temperature overnight, the mixture was concentrated under reduced pressure. Ethyl acetate (250 mL) was added to the residue and the resulting precipitate was separated by filtration. The filtrate was washed quickly with ice-cold satd $NaHCO_3$ solution (250 mL) and H_2O (250 mL×3), dried over Na_2SO_4 and concentrated. The residue was purified by column chromatography on silica gel eluted with EtOAc/hexanes (1:1, v/v, R_f = 0.45) to give 1,3-bis(4-cyanobenzoyl)-1,3-diazepan-2-one (0.86 g, 40%) as a white solid (mp 219–221 °C). ^{1}H NMR (300 MHz, DMSO-d_6) δ 7.85 (4H, d, J = 8.1 Hz), 7.65 (4H, d, J = 8.1 Hz), 4.21 (4H, m), 1.88 (4H, m); APT ^{13}C NMR (75.5 MHz, DMSO-d_6) δ 170.6 (up), 159.8 (up), 140.4 (up), 133.2 (down), 128.7 (down), 119.0 (up), 114.1 (up), 45.4 (up), 27.2 (up); CI–MS *m/e* 373 $(M+1)^+$; IR ($CHCl_3$, cast) ν 2230, 1692 cm^{-1}. Anal. calcd for $C_{21}H_{16}N_4O_3$: C, 67.73; H, 4.33; N, 15.05. Found: C, 67.72; H, 4.35; N, 14.98.

1,3-Bis(3-cyanobenzoyl)-[1,3]-diazepan-2-one (4). **4** was prepared by the same method described above for the synthesis of **9** using **3** as starting material (45% from **3**, mp 204–205 °C). ^{1}H NMR (300 MHz, DMSO-d_6) δ 7.97–7.56 (8H, m), 4.24 (4H, bs), 1.88 (4H, bs); APT ^{13}C NMR (75.5 MHz, DMSO-d_6) δ 170.2 (up), 159.9 (up), 137.6 (up), 135.4 (down), 132.5 (down), 131.4 (down), 130.5 (down), 118.9 (up), 112.4 (up), 45.5 (up), 27.2 (up); CI–MS 373 $(M+1)^+$; IR ($CHCl_3$, cast) ν 2233, 1691 cm^{-1}. Anal. calcd for $C_{21}H_{16}N_4O_3$: C, 67.73; H, 4.33; N, 15.05. Found: C, 67.45; H, 4.38; N, 14.89.

1,3-Bis(4-thiocarbamylbenzoyl)-[1,3]-diazepan-2-one (10). Several drops of H_2O were added to a suspension of **9** (0.8 g, 2.2 mmol) in diethyl dithiophosphate (3 mL). The reaction mixture was stirred at room temperature for 2 days, and then quenched with H_2O (50 mL). The resulting precipitate was filtered and washed with a large volume of H_2O, EtOAc (10 mL) and hexanes (50 mL) to give 1,3-bis(4-thiocarbamylbenzoyl)-1,3-diazepan-2-one (0.9 g, 95%) as a yellow powder (mp 235–238 °C). ^{1}H NMR (300 MHz, DMSO-d_6) δ 9.98 (2H, s), 9.57 (2H, s), 7.81 (4H, d, J = 8.1 Hz), 7.50 (4H, d, J = 8.1 Hz), 4.21 (4H, m), 1.87 (4H, m); APT ^{13}C NMR (75.5 MHz, DMSO-d_6) δ 200.1 (up), 171.5 (up), 160.0 (up), 142.4 (up), 138.3 (up), 128.0 (down), 127.6 (down), 45.3 (up), 27.6 (up); CI–MS *m/e* 373 $(M+1-2H_2S)^+$. Anal. calcd for $C_{21}H_{20}N_4O_3S_2 0.4H_2O$: C, 56.33; H, 4.68; N, 12.51; S, 14.32. Found: C, 56.64; H, 4.62; N, 12.34; S, 14.37.

1,3-Bis(3-thiocarbamylbenzoyl)-[1,3]-diazepan-2-one (5). **5** was prepared by the same methods described above for the synthesis of **10** using **4** as starting material (95% from **4**, mp 228–230 °C). ^{1}H NMR (300 MHz, DMSO-d_6) δ 9.99 (2H, s), 9.61 (2H, s), 8.02–7.41 (8H, m), 4.24 (4H, bs), 1.89 (4H, bs); APT ^{13}C NMR (75.5 MHz, DMSO-d_6) δ 199.5 (up), 171.5 (up), 160.1 (up), 139.9 (up), 135.8 (up), 130.6 (down), 130.3 (down), 128.9 (down), 127.3 (down), 45.4 (up), 27.6 (up); CI–MS *m/e* 373 $(M+1-2H_2S)^+$. Anal. calcd for $C_{21}H_{20}N_4O_3S_2$: C, 57.25; H, 4.58; N, 12.72; S, 14.56. Found: C, 56.96; H, 4.60, N, 12.45; S, 14.56.

1,3-Bis(3-amidinobenzoyl)-[1,3]-diazepan-2-one (2). A suspension of **5** (230 mg, 0.523 mmol) in acetone (10 mL) was treated with MeI and the yellow mixture was heated to reflux for 1 h. The resulting brown mixture was concentrated under reduced pressure to give the crude product **6** that was used for the next step without further purification.

The brown solid was suspended in ice-cold anhydrous acetonitrile (15 mL) and treated with ammonium acetate (85 mg, 1.1 mmol) at 0 °C. The reaction mixture was stirred at room temperature overnight and turned to a white cloudy mixture. The resulting precipitate was filtered out, washed with ice-cold acetonitrile and ethyl ether, and dried under vacuum to give 1,3-bis(3-amidi-

nobenzoyl)-1,3-diazepan-2-one, hydroiodide salt (220 mg, 64%) as a white powder (mp 243–245 °C). ^{1}H NMR (300 MHz, DMSO-d_6) δ 9.20 (6H, bs), 7.88–7.60 (8H, m), 4.26 (4H, bs), 1.91 (4H, bs); APT ^{13}C NMR (75.5 MHz, DMSO-d_6) δ 170.9 (up), 165.4 (up), 160.0 (up), 136.9 (up), 132.8 (down), 131.5 (down), 129.9 (down), 129.2 (up), 127.5 (down), 45.6 (up), 27.5 (up). Anal. calcd for $C_{21}H_{22}N_6O_3 \cdot 1.9HI \cdot 0.4CH_3COOH$): C, 38.88; H, 3.82; N, 12.48. Found: C, 39.14; H, 3.80; N, 12.52.

1,3-Bis(4-*N*-hydroxyamidinobenzoyl)-[1,3]-diazepan-2-one (12). **11** was prepared by the method described above for the synthesis of **6** using **10** (250 mg, 0.57 mmol) as starting material. The brown solid was dissolved in anhydrous DMF (10 mL). At 0 °C, Et_3N (0.18 mL, 1.25 mmol) and $NH_2OH \cdot HCl$ (90 mg, 1.25 mmol) were added respectively. The reaction mixture was stirred at room temperature overnight, then neutralized with Et_3N (0.18 mL, 1.25 mmol) and diluted with ethyl acetate. The organic phase was washed with H_2O, dried over Na_2SO_4 and passed through a short silica gel column. After concentrating under vacuum, 1,3-bis(4-*N*-hydroxyamidinobenzoyl)-1,3-diazepan-2-one (170 mg, 68%) was collected as a white powder (mp > 280 °C dec). ^{1}H NMR (300 MHz, DMSO-d_6) δ 9.82 (2H, s), 7.67 (4H, d, J = 8.4 Hz), 7.48 (4H, d, J = 8.4 Hz), 5.86 (4H, s), 4.22 (4H, bs), 1.86 (4H, bs); APT ^{13}C NMR (75.5 MHz, DMSO-d_6) δ 171.8 (up), 160.1 (up), 151.0 (up), 136.8 (up), 136.3 (up), 128.0 (down), 126.1 (down), 45.4 (up), 27.6 (up). Anal. calcd for $C_{21}H_{22}N_6O_5$: C, 57.53; H, 5.05; N, 19.17. Found: C, 57.85; H, 5.26; N, 19.05.

1,3-Bis(4-*N*-acetoxyamidinobenzoyl)-[1,3]-diazepan-2-one (13). **12** (150 mg, 0.34 mmol) was dissolved in DMF (3 mL). At 0 °C, Et_3N (105 μL, 0.75 mmol) and CH_3COCl (55 μL, 0.75 mmol) were added, respectively. The reaction mixture was stirred at room temperature overnight, then diluted with ethyl acetate and washed with H_2O. The organic phase was dried over Na_2SO_4 and then concentrated under vacuum. The residue was purified by column chromatography on silica gel eluted with EtOAc/hexanes (v/v = 2:1, R_f = 0.65) to give 1,3-bis(4-*N*-acetoxyamidinobenzoyl)-1,3-diazepan-2-one (160 mg, 90%) as a white solid (mp > 280 °C dec). ^{1}H NMR (300 MHz, DMSO - d_6) δ 7.69 (4H, d, J = 8.0 Hz), 7.54 (4H, d, J = 8.0 Hz), 6.87 (4H, s), 4.22 (4H, bs), 2.12 (6H, s), 1.88 (4H, bs); APT ^{13}C NMR (75.5 MHz, DMSO-d_6) δ 171.6 (up), 169.3 (up), 156.6 (up), 138.0 (up), 134.9 (up), 128.0 (down), 127.6 (down), 45.3 (up), 27.5 (up), 20.7 (down). Anal. calcd for $C_{25}H_{26}N_6O_7 \, H_2O$: C, 55.55; H, 5.22; N, 15.55. Found: C, 55.37; H, 5.09; N, 15.80.

3,3,6,6-Tetramethylcycloheptanone (15).[35,36] At 0 °C, to a stirred suspension of cuprous bromide–dimethyl sulfide complex (1.4 g, 6.8 mmol) in ether (15 mL) was added dropwise, an ethereal solution of methyllithium (11.5 mL, 1.4 M, 16.1 mmol) resulting in a colorless solution. After stirring for 5 min, a solution of **14**[41] (1.0 g, 6.5 mmol) in ether (15 mL) was added dropwise after which the reaction mixture, from which yellow precipitate was formed, was stirred at room temperature for 40 min, then poured into 100 mL NH_4Cl/NH_4OH buffer (pH ≈8). The aqueous phase was extracted with ether (3×50 mL). The combined extracts were washed with saturated aqueous NaCl and dried (Na_2SO_4). After concentration under reduced pressure, **15** (1.08 g, 99%) was collected as a colorless liquid.[13] ^{1}H NMR ($CDCl_3$) δ 2.36 (4H, s), 1.55 (4H, s), 1.00 (12H, s); ^{13}C NMR (75.5 MHz, $CDCl_3$) δ 212.0, 57.2, 37.7, 32.1, 30.2; ES–MS m/e 169.1 $(M+1)^+$.

3,3,6,6 - Tetramethyl - 1 - trimethylsilyloxycycloheptene (24). Standard protocol for the formation of trimethylsilylenol ethers. Sodium iodide was heated to 140 °C for 3 h then dissolved in acetonitrile to give a 1 M solution. Chlorotrimethylsilane (3.9 mL, 30.8 mmol) was added dropwise at 0 °C to a stirred mixture of **15** (3.45 g, 20.5 mmol) and triethylamine (8.6 mL, 61.5 mmol). After warming to room temperature the above sodium iodide solution (26 mL, 26 mmol) was added dropwise to the reaction mixture resulting in an exothermic reaction and the formation of a white precipitate in the light brown solution. After stirring overnight the reaction was quenched by addition of ice-water and extracted with pentane. The extracts were quickly washed sequentially with ice-cold saturated aqueous solutions of ammonium chloride and sodium hydrogen carbonate, then with brine, dried (Na_2SO_4) and concentrated under reduced pressure to give the silyl enol ether as a brown liquid (4.86 g, 99%). ^{1}H NMR ($CDCl_3$) δ 4.69 (1H, s), 2.08 (2H, s), 1.45 (4H, m), 0.99 (6H, s), 0.95 (6H, s), 0.16 (9H, s). No further purification was attempted on this compound which was used directly in the next step.

1-Trimethylsilyloxy-3,3,5,5-tetramethylcyclohexene (18). This was prepared by the general protocol for the formation of trimethylsilyl enol ethers in 99% yield from 3,3,5,5-tetramethylcyclohexanone[42,43] (**17**). ^{1}H NMR ($CDCl_3$) δ 4.66 (1H, s), 1.76 (2H, s), 1.26 (2H, s), 1.00 (6H, s), 0.98 (6H, s), 0.18 (9H, s). No further purification was attempted on this compound which was used directly in the next step.

2-[(*Z*)-*p*-Cyanobenzylidene]-3,3,5,5-tetramethylcyclohexanone (20). At 0 °C, to a solution of **18** (226 mg, 1.0 mmol) and **19**[44,45] (190 mg, 1.1 mmol) in dichloromethane (5 mL) was added dropwise, a solution of $TiCl_4$ in dichloromethane (1.2 mL, 1.0 M, 1.2 mmol). The resulting dark mixture was stirred at room temperature overnight, then quenched with water (3 mL). The aqueous phase was extracted with ethyl acetate (3×5 mL) and the combined extracts were washed with saturated aqueous NaCl, dried (Na_2SO_4) and concentrated under reduced pressure. The residue was purified by column chromatography to give **16** (40 mg, 10%) and the title product, **20** (180 mg, 67%) as a yellow liquid which turned to a wax-like solid on standing. Mp 55–58 °C; ^{1}H NMR ($CDCl_3$) δ 7.54 (2H, d, J = 6.2 Hz), 7.32 (2H, d, J = 6.3 Hz), 6.39 (1H, s), 2.43 (2H, s), 1.73 (2H, s), 1.26 (6H, s), 1.11 (6H, s); IR ($CHCl_3$, cast) ν 2225, 1734, 1694, 1603 cm^{-1}. No further purification was attempted on this compound which was used directly in the next step.

On exposure to ambient laboratory light for more than one week, **20** was converted into a mixture of *E*- and

Z-isomers. Separation of the isomers by column chromatography was difficult due to their close R_f values. The NMR spectrum of the *E*-isomer was obtained from a mixture with the *Z*-isomer. ^{1}H NMR ($CDCl_3$) δ 7.53 (2H, d, $J=8.4$ Hz), 7.31 (2H, d, $J=8.1$ Hz), 6.38 (1H, s), 2.42 (2H, s), 1.72 (2H, s), 1.26 (6H, s), 1.11 (6H, s).

1-Trimethylsilyloxy-2-(*p*-cyanobenzylidene)-3,3,5,5-tetramethyl-cyclohexanone (21). This was obtained in 95% yield from **20** by the standard protocol for the formation of trimethylsilyl enol ethers. ^{1}H NMR ($CDCl_3$) δ 7.50 (2H, d, $J=8.3$ Hz), 7.29 (2H, d, $J=8.5$ Hz), 6.28 (1H, s), 4.94 (1H, s), 1.53 (2H, s), 1.24 (6H, s), 1.11 (6H, s), −0.19 (9H, s). No further purification was attempted on this compound which was used directly in the next step.

2,6-Bis[(*Z*)-*p*-cyanobenzylidene]-3,3,5,5-tetramethylcyclohexanone (16). At 0 °C, to a solution of **21** (210 mg, 0.62 mmol) and **8a**[44,45] (120 mg, 0.68 mmol) in dichloromethane (5 mL) was added dropwise a solution of $TiCl_4$ in dichloromethane (0.75 mL, 1.0 M, 0.75 mmol). The resulting dark mixture was heated at reflux for 3 h, and then quenched with water (3 mL). The aqueous phase was extracted with ethyl acetate (3×5 mL) and the combined extracts were washed with brine, dried (Na_2SO_4) and concentrated under reduced pressure. The residue was purified by column chromatography to give **16** (145 mg, 62%) as a yellow solid. Mp 151–154 °C; ^{1}H NMR ($CDCl_3$) δ 7.43 (4H, d, $J=8.3$ Hz), 7.25 (4H, d, $J=8.1$ Hz), 6.60 (2H, s), 1.82 (2H, s), 1.33 (12H, s); ^{13}C NMR ($CDCl_3$) δ 197.0, 151.3, 141.2, 132.0, 130.0, 129.5, 119.1, 111.4, 52.9, 38.8, 31.3; ES–MS *m*/*e* 381.2 $(M+1)^+$; IR (cast) ν 2229, 1676, 1615 cm^{-1}. Anal. calcd for $C_{26}H_{24}N_2O$ $0.2H_2O$: C, 81.31; H, 6.40; N, 7.29. Found: C, 81.56; H, 6.30; N, 7.23.

On exposure to ambient laboratory light for more than one week, **16** was converted into a mixture of *Z*,*Z*- and *Z*,*E*-isomers. The separation of the isomers by column chromatography was difficult due to their close R_f values. The ^{1}H NMR spectrum of the *Z*,*E*-isomer was therefore obtained from a mixture with the *Z*,*Z*-isomer. ^{1}H NMR ($CDCl_3$) δ 7.62–7.23 (8H, m), 6.61 (1H, s), 6.60 (1H, s), 1.69 (2H, s), 1.32 (6H, s), 1.13 (6H, s).

2,6-Bis[(*Z*)-*p*-amidinobenzylidene]-3,3,5,5-tetramethylcyclohexanone (31). Dry HCl gas was passed at 0 °C through a solution of **21** (100 mg, 0.26 mmol) in anhydrous ethyl ether (5 mL) and methanol (2 mL) for 5 min. The reaction vessel was then sealed and stored at 0 °C for 2 days. After removal of the solvents under reduced pressure, the residue was dissolved in methanol and treated with ammonium acetate (25 mg, 0.31 mmol) at 0 °C followed by stirring at room temperature overnight. The resulting mixture was diluted with water to a final volume of 5 mL. Ten 50-μL aliquots of this solution were purified by semi-preparative HPLC (Beckman Ultrasphere C-18 column) using a 25–30% gradient of solvent A (0.1% TFA in acetonitrile) in solvent B (0.1% TFA in water) to give **31** (12 mg, 70% from **16**), which was collected as a white solid after concentration under vacuum. Mp 185–187 °C; ^{1}H NMR (methanol-d_4) δ 7.63 (4H, d, $J=8.4$ Hz), 7.43 (4H, d, $J=8.4$ Hz), 6.86 (2H, s), 1.90 (2H, s), 1.39 (12H, s); ^{13}C NMR (methanol-d_4) δ 211.7, 166.9, 151.2, 143.2, 129.9, 129.8, 127.5, 127.0, 52.4, 38.1, 30.3; ES–MS *m*/*e* 415.3 $(M+1)^+$. Anal. calcd for $C_{26}H_{30}N_4O{\cdot}2CF_3COOH{\cdot}0.5H_2O$: C, 55.30; H, 5.10; N, 8.60. Found: C, 55.30; H, 5.40; N, 8.76.

2,6-Bis[(Z)-*m*-cyanobenzylidene]-3,3,5,5-tetramethylcyclohexanone (23). This was prepared in 50% yield from **18** and 3-dimethoxymethyl-benzonitrile[46,47] by the method described above for the synthesis of **16**. Mp 107–108 °C; ^{1}H NMR ($CDCl_3$) δ 7.47–7.20 (8H, m), 6.55 (2H, s), 1.80 (2H, s), 1.31 (12H, s); ^{13}C NMR ($CDCl_3$) δ 197.1, 150.9, 137.3, 133.5, 132.5, 131.3, 128.9, 128.2, 118.8, 112.3, 52.6, 38.6, 31.1; ES–MS *m*/*e* 381.2 $(M+1)^+$. Anal. calcd for $C_{26}H_{24}N_2O$: C, 82.07; H, 6.36; N, 7.36. Found: C, 82.20; H, 6.51; N, 7.34.

2,6-Bis[(*Z*)-*m*-amidinobenzylidene]-3,3,5,5-tetramethylcyclohexanone (33). This was prepared in 70% yield from **23** by the method described above for the synthesis of **31**. Mp 170–173 °C; ^{1}H NMR (methanol-d_4) δ 7.71–7.26 (8H, m), 6.83 (2H, s), 1.86 (2H, s), 1.38 (12H, s); ^{13}C NMR (methanol-d_4) δ 209.3, 162.3, 151.2, 138.1, 134.2, 129.6, 128.9, 128.6, 126.8, 121.9, 52.2, 38.4, 30.4; ES–MS *m*/*e* 208.2 $1/2(M+2)^{2+}$, 415.3 $(M+1)^+$. Anal. calcd for $C_{26}H_{30}N_4O{\cdot}2CF_3COOH{\cdot}0.75H_2O$: C, 54.92; H, 5.15; N, 8.54. Found: C, 55.02; H, 5.30; N, 8.95.

2-[(*Z*)-*m*-Cyanobenzylidene]-6-[(*Z*)-*p*-cyanobenzylidene]-3,3,5,5-tetramethylcyclohexanone (22). This was prepared in 65% yield from **21** and 3-dimethoxymethyl-benzonitrile[46,47] by the method described above for the synthesis of **16**. Mp 142–143 °C; ^{1}H NMR ($CDCl_3$) δ 7.51–7.17 (8H, m), 6.56 (1H, s), 6.55 (1H, s), 1.80 (2H, s), 1.32 (12H, s); ^{13}C NMR ($CDCl_3$) δ 197.4, 151.6, 151.3, 141.1, 137.6, 133.7, 133.0, 132.0, 131.4, 129.9, 129.0, 128.9, 128.3, 119.2, 118.9, 112.6, 111.4, 52.9, 39.0, 38.9, 31.3, 31.3; ES–MS *m*/*e* 381.2 $(M+1)^+$. Anal. calcd for $C_{26}H_{24}N_2O{\cdot}0.6H_2O$: C, 79.81; H, 6.49; N, 7.16. Found: C, 79.64; H, 6.23; N, 7.41.

2-[(*Z*)-*m*-Amidinobenzylidene]-6-[(*Z*)-*p*-amidinobenzylidene]-3,3,5,5-tetramethylcyclohexanone (32). This was prepared in 56% yield from **22** by the method described above for the synthesis of **31**. Mp 163–165 °C; ^{1}H NMR (methanol-d_4) δ 7.70–7.30 (8H, m), 6.84 (2H, s), 1.87 (2H, s), 1.37 (12H); ^{13}C NMR (methanol-d_4) δ 212.4, 165.7, 164.4, 153.5, 151.2, 150.8, 138.3, 134.2, 133.9, 132.9, 130.1, 129.8, 128.9, 128.5, 127.4, 126.7, 52.3, 38.1, 30.4; ES–MS *m*/*e* 208.3 $1/2(M+2)^{2+}$, 415.3 $(M+1)^+$. Anal. calcd for $C_{26}H_{30}N_4O{\cdot}2CF_3COOH{\cdot}0.5H_2O$: C, 55.30; H, 5.10; N, 8.60. Found: C, 55.44; H, 5.52; N, 8.77.

2-[(*Z*)-*p*-Cyanobenzylidene]-3,3,6,6-tetramethylcycloheptanone (26). A solution of $TiCl_4$ in dichloromethane (2.0 mL, 1.0 M, 2.0 mmol) was added dropwise at room temperature to a solution of **24** (240 mg, 1.0 mmol) and **25**[48] (530 mg, 3.0 mmol) in 1,2-dichloroethane (3 mL) in a flask equipped with a reflux condenser. The resulting dark mixture was heated at reflux overnight, then cooled to room temperature and quenched with water (10 mL)

and the aqueous phase was extracted with ethyl acetate (3×10 mL). The combined organic layers were washed with brine, dried (Na_2SO_4) and concentrated under reduced pressure. The residue was purified by column chromatography to give **28** (20 mg, 5%) as a yellow solid and the title product, **26** (113 mg, 41%) as a yellow oil which turned to a wax-like solid on standing. Mp 84–85 °C; ^{1}H NMR ($CDCl_3$) δ 7.55 (2H, d, J = 6.3 Hz), 7.31 (2H, d, J = 6.2 Hz), 6.33 (1H, s), 2.19 (2H, s), 1.51 (4H, m), 1.24 (6H, s), 0.97 (6H, s); ^{13}C NMR ($CDCl_3$) δ 210.9, 158.0, 140.9, 132.6, 129.2, 122.7, 119.2, 111.2, 57.6, 37.9, 37.4, 37.0, 33.9, 29.9, 29.4; ES–MS m/e 282.2 $(M+1)^+$. No further purification was attempted on this compound which was used directly in the next step.

1-Trimethylsilyloxy-2-[(*Z*)-*p*-cyanobenzylidene]-3,3,6,6-tetramethylcycloheptanone (27). This was prepared in quantitative yield by the standard protocol for the formation of trimethylsilyl enol ethers. ^{1}H NMR ($CDCl_3$) δ 7.53 (2H, d, J = 7.6 Hz), 7.24 (2H, d, J = 7.6 Hz), 6.26 (1H, s), 4.69 (1H, s), 1.50 (4H, m), 1.19 (6H, s), 1.02 (6H, s), 0.05 (9H, s). No further purification was attempted on this compound which was used directly in the next step.

2,7-Bis[(*Z*)-*p*-cyanobenzylidene]-3,3,6,6-tetramethylcycloheptanone (28). This was prepared in 43% yield from **27** by the method described above for the synthesis of **26**. Mp 167–168 °C; ^{1}H NMR ($CDCl_3$) δ 7.34 (4H, d, J = 5.0 Hz), 7.13 (4H, d, J = 4.9 Hz), 6.48 (2H, s), 1.76 (4H, s), 1.28 (12H, s); ^{13}C NMR ($CDCl_3$) δ 200.8, 153.5, 141.0, 130.9, 129.8, 128.1, 118.8, 110.9, 38.5, 38.0, 29.3; ES–MS m/e 395.2 $(M+1)^+$; IR ($CHCl_3$, cast) ν 2226, 1668, 1604 cm^{-1}. Anal. calcd for $C_{27}H_{26}N_2O{\cdot}0.75H_2O$: C, 79.48; H, 6.79; N, 6.87. Found: C, 79.48; H, 6.53; N, 6.79.

2,7-Bis[(Z)-*p*-amidinobenzylidene)]-3,3,6,6-tetramethylcycloheptanone (34). This was prepared in 65% yield from **28** by the method described above for the synthesis of **31**. Mp 205–207 °C; ^{1}H NMR (methanol-d_4) δ 7.52 (4H, d, J = 8.4 Hz), 7.30 (4H, d, J = 8.4 Hz), 6.71 (2H, s), 1.81 (4H, s), 1.29 (12H, s); ^{13}C NMR (methanol-d_4) δ 212.8, 166.6, 153.7, 143.4, 129.9, 129.3, 127.4, 126.4, 38.7, 38.4, 28.5; ES–MS m/e 215.3 $1/2(M+2)^{2+}$, 429.2 $(M+1)^+$; FABHRMS m/e 429.2652 $(M+H)^+$, calcd for $C_{27}H_{33}N_4O$ 429.2654. Anal. calcd for $C_{27}H_{32}N_4O{\cdot}2.75CF_3COOH{\cdot}2.5H_2O$: C, 49.59; H, 5.09; N, 7.12. Found: C, 49.62; H, 4.92; N, 7.10.

2-[(*Z*)-*m*-Cyanobenzylidene]-7-[(*Z*)-*p*-cyanobenzylidene]-3,3,6,6-tetramethylcycloheptanone (35). This was prepared in 34% yield from **27** and 3-dimethoxymethyl-benzonitrile[48] by the method described above for the synthesis of **26**. Mp 125–127 °C; ^{1}H NMR ($CDCl_3$) δ 7.56–7.06 (8H, s), 6.45 (1H, s), 6.40 (1H, s), 1.74 (4H, s), 1.27 (6H, s), 1.25 (6H, s); ES–MS m/e 395.3 $(M+1)^+$. Anal. calcd for $C_{27}H_{26}N_2O{\cdot}0.3H_2O$: C, 81.09; H, 6.70; N, 7.00. Found: C, 81.09; H, 6.43; N, 7.20.

2-[(*Z*)-*m*-Amidinobenzylidene]-7-[(*Z*)-*p*-amidinobenzylidene]-3,3,6,6-tetramethylcycloheptanone (36). This was prepared from **35** in 62% yield by the method described above for the synthesis of **31**. Mp 176–179 °C; ^{1}H NMR (methanol-d_4) δ 7.88–7.25 (8H, m), 6.73 (1H, s), 6.72 (1H, s), 1.82 (4H, s), 1.30 (6H, s), 1.29 (6H, s); ^{13}C NMR (methanol-d_4) δ 190.5, 153.6, 153.0,143.4, 138.5, 138.1, 134.2, 130.6, 129.8, 129.7, 129.4, 128.9, 128.8, 128.1, 127.4, 126.7, 126.4, 38.8, 38.8, 38.5, 38.3, 28.6, 28.3; ES–MS m/e 215.2 $1/2(M+2)^{2+}$, 429.3 $(M+1)^+$; FABHRMS m/e 429.2652 $(M+H)^+$, calcd for $C_{27}H_{33}N_4O$ 429.2654. Anal. calcd for $C_{27}H_{32}N_4O{\cdot}1.7CF_3COOH{\cdot}0.75H_2O$: C, 57.42; H, 5.58; N, 8.81. Found: C, 57.49; H, 5.52; N, 8.89.

2-[(*Z*)-*m*-Cyanobenzylidene]-3,3,6,6-tetramethylcycloheptanone (37). This was prepared in 32% yield from **24** and 3-dimethoxymethyl-benzonitrile[46,47] by the method described above for the synthesis of **26**. Mp 65–68 °C; ^{1}H NMR ($CDCl_3$) δ 7.50–7.34 (4H, m), 6.31 (1H, s), 2.19 (2H, s), 1.58–1.49 (4H, m), 1.24 (6H, s), 0.98 (6H, s); ES–MS m/e 282.1 $(M+1)^+$. No further purification was attempted on this compound which was used directly in the next step.

2,7-Bis[(*Z*)-*m*-cyanobenzylidene]-3,3,6,6-tetramethylcycloheptanone (38). was prepared in 30% yield from **24** and 3-dimethoxymethyl-benzonitrile[46,47] by the method described above for the synthesis of **26**. Mp 157–160 °C; ^{1}H NMR ($CDCl_3$) δ 7.39–7.13 (8H, m), 6.42 (2H, s), 1.76 (4H, s), 1.28 (12H, s); ^{13}C NMR ($CDCl_3$) δ 201.4, 153.8, 137.6, 133.9, 132.8, 131.1, 128.9, 127.3, 119.0, 112.3, 38.6, 38.5, 29.7. Anal. calcd for $C_{27}H_{26}N_2O{\cdot}0.4H_2O$: C, 80.73; H, 6.72; N, 6.97. Found: C, 80.67; H, 6.65; N, 6.97.

2,7-Bis[(*Z*)-*m*-amidinobenzylidene]-3,3,6,6-tetramethylcycloheptanone (39). was prepared in 59% yield from **38** by the method described above for the synthesis of **31**. Mp 194–196 °C; ^{1}H NMR (methanol-d_4) δ 7.67–7.21 (8H, m), 6.72 (2H, s), 1.81 (4H, s), 1.30 (12H, s); ^{13}C NMR (methanol-d_4) δ 208.7, 161.8, 153.1, 138.4, 134.2, 129.4, 129.0, 128.8, 128.1, 126.5, 38.6, 38.4, 28.6; ES–MS m/e 215.2 $1/2(M+2)^{2+}$, 429.3 $(M+1)^+$; FABHRMS m/e 429.2634 $(M+H)^+$, calcd for $C_{27}H_{33}N_4O$ 429.2654 Anal. calcd for $C_{27}H_{32}N_4O{\cdot}1.9CF_3COOH{\cdot}H_2O$: C, 55.78; H, 5.46; N, 8.45. Found: C, 56.01; H, 5.66; N, 8.27.

Enzyme assays

Human FXa was obtained from American Diagnostica Inc., Greenwich, CT, USA. Human thrombin, bovine trypsin and human plasmin were from Sigma, St. Louis, MO, USA. The activities of human FXa, human thrombin, bovine trypsin and human plasmin were determined as the initial rates of the cleavage of peptide *p*-nitroanilide by the enzymes. Initial rates for the control assays (no inhibitor) were measured at different substrate concentrations and used in the Michaelis–Menten equation to determine K_m and v_{max}[39] under the present assay conditions (TableCurve 2D Windows v4.07 from AISN Software, Inc.). Competitive inhibition was assumed, and initial rates for the inhibition assays were measured at different inhibitor concentrations and K_i values were calculated using Dixon analysis.[40] Data analysis was performed with the commercial graphing package Origin 5.0 (Microcal Software, Inc.). The assay was performed at 37 °C in semimicrocuvette. Reaction rates were determined by measuring the rate of the absorbance change at 405 nM in

a Beckman 2400 spectrophotometer or a Shimadzu UV-2401PC UV–vis recording spectrophotometer.

Anti-FXa activity

Anti-FXa activities were measured by using the chromogenic substrate MeO-CO-D-CHG-Gly-Arg-*p*NA (American Diagnostica Inc.) and human FXa. DMSO (20 μL) or a DMSO solution of the inhibitor (20 μL) and a solution of substrate (100 μL) were mixed with 0.1 M Tris–0.2 M NaCl buffer pH 8.4 (360 μL). The reaction was started with the addition of 0.31 unit/mL (or 7.0 nM) human FXa solution (20 μL). The inhibition assays were run with 350 μM substrate concentration.

Anti-thrombin activity

Anti-thrombin activities were measured by using the chromogenic substrate *N*-*p*-tosyl-Gly-Pro-Arg-*p*NA (Sigma) and human thrombin. DMSO (15 μL) or a DMSO solution of the inhibitor (15 μL) and a solution of substrate (15 μL) were mixed with 0.14 M NaCl–5 mM KCl–30 mM HEPES–125 μM PEG-8000 pH 7.4 (405 μL). The reaction was started with the addition of 0.1 unit/mL (or 2.7 nM) human thrombin solution (15 μL). The inhibition assays were run with 20.1 μM substrate concentration.

Anti-trypsin activity

Anti-trypsin activities were measured by using chromogenic substrate *N*-*p*-tosyl-Gly-Pro-Arg-*p*NA (Sigma) and bovine trypsin. DMSO (15 μL) or a DMSO solution of the inhibitor (15 μL) and a solution of substrate (15 μL) were mixed with 0.14 M NaCl–5 mM KCl–30 mM HEPES–125 μM PEG-8000 pH 7.4 (405 μL). The reaction was started with the addition of 4.2 nM bovine trypsin solution (15 μL). The inhibition assays were run with 40.2 μM substrate concentration.

Anti-plasmin activity

Anti-plasmin activities were measured by using chromogenic substrate D-Val-Leu-Lys-*p*NA (Sigma) and human plasmin. DMSO (15 μL) or a DMSO solution of the inhibitor (15 μL) and a solution of substrate (15 μL) were mixed with 0.14 M NaCl–5 mM KCl–30 mM HEPES–125 μM PEG-8000 pH 7.4 (405 μL). The reaction was started with the addition of 0.1 unit/mL human plasmin solution (15 μL). The inhibition assays were run with both 302 μM and 206 μM substrate concentration.

X-ray crystallographic analysis

Data were processed and the structures were refined on *F* using the XTAL 3.7[49] suite of programs. The structures were solved using SHELXS-86[50] in the *Pcan* space group. All non-hydrogen atoms were refined with anisotropic thermal parameters. Hydrogen atoms were located in idealized positions based on the carbon backbone and were given a fixed isotropic thermal parameter $U = 0.070$.

Molecular modeling

We utilized the X-ray protein structure coordinates of human FXa reported by Padmanabhan et al.[24] (PDB accession code: 1hcg). The standard chymotrypsinogen residue numbering[51] was maintained. Comparative conformational energies were calculated by first building the molecular model in Sybyl (Tripos, Inc.), then optimizing the geometry using the AM1 module in Gaussian98 (Gaussian, Inc.), and doing final geometry optimization/energy minimization using the Gaussian 94/98 (3,21) basis set. Docking calculations utilized the Autodock program developed by Olson and colleagues[25,26] (The Scripps Research Inst) with 10 docking runs for each ligand. Grid maps were centered on the active site of FXa with a grid-point spacing of 0.375 Å and 61×61×61 points in the grid maps. The genetic algorithm docking method was used with a population size of 50; 2.5 10^6 energy evaluations; 2.7 10^4 maximum number of generations; an elitism value of 1; a mutation rate of 0.02; a crossover rate of 0.80; a GA window size = 10; and cauchy distribution parameters, alpha = 0 and beta = 1.

Supporting Information available

Tables of ^{1}H and NOESY data for **16**, **22**, **23**, **28**, **35** and **38**; elemental analyses for compounds **2**–**5**, **8**, **9**, **12**, **13**, **16**, **22**, **23**, **28**, **31**–**36**, **38** and **39**; crystallographic data for **9** and **28**. This material is available free of charge via the Internet at http://www.elsevier.com.

Acknowledgements

Supported in part by grants from the NIH and American Heart Association Midwest Affiliate. We thank Dr. Bernard Santarsiero for assistance with the Ortep plots and small molecule crystallographic data conversion.

References and Notes

1. Rai, R.; Sprengeler, P. A.; Elrod, K. C.; Young, W. B. *Curr. Med. Chem.* **2001**, *8*, 101.
2. Vacca, J. P. *Annu. Rep. Med. Chem.* **1998**, *33*, 81.
3. Vacca, J. P. *Curr. Opin. Chem. Biol.* **2000**, *4*, 394.
4. Zhu, B. Y.; Scarborough, R. M. *Annu. Rep. Med. Chem.* **2000**, *35*, 83.
5. Fevig, J. M.; Wexler, R. R. *Annu. Rep. Med. Chem.* **1999**, *34*, 81.
6. Hauptmann, J.; Sturzebecher, J. *Thromb. Res.* **1999**, *93*, 203.
7. Ripka, W. C.; Vlasuk, G. P. *Annu. Rep. Med. Chem.* **1997**, *32*, 71.
8. Vlasuk, G. P. *Thromb. Haemost.* **1993**, *70*, 212.
9. Hauptmann, J.; Kaiser, B. *Blood Coagul. Fibrinolysis* **1993**, *4*, 577.
10. Lapatto, R.; Krengel, U.; Schreuder, H. A.; Arkema, A.; de Boer, B.; Kalk, K. H.; Hol, W. G.; Grootenhuis, P. D.; Mulders, J. W.; Dijkema, R.; Theunissen, H. J.; Dijkstra, B. W. *EMBO J.* **1997**, *16*, 5151.
11. Stassens, P.; Bergum, P. W.; Gansemans, Y.; Jespers, L.; Laroche, Y.; Huang, S.; Maki, S.; Messens, J.; Lauwereys, M.; Cappello, M.; Hotez, P. J.; Lasters, I.; Vlasuk, G. P. *Proc. Natl. Acad. Sci. U.S.A.* **1996**, *93*, 2149.

12. Fioravanti, C.; Burkholder, D.; Francis, B.; Siegl, P. K.; Gibson, R. E. *Thromb. Res.* **1993**, *71*, 317.
13. Lynch, J. J., Jr.; Sitko, G. R.; Lehman, E. D.; Vlasuk, G. P. *Thromb. Haemost.* **1995**, *74*, 640.
14. Nicolini, F. A.; Lee, P.; Malycky, J. L.; Lefkovits, J.; Kottke-Marchant, K.; Plow, E. F.; Topol, E. J. *Blood Coagul. Fibrinolysis* **1996**, *7*, 39.
15. Sato, K.; Taniuchi, Y.; Kawasaki, T.; Hirayama, F.; Koshio, H.; Matsumoto, Y.; Iizumi, Y. *Jpn. J. Pharmacol.* **1998**, *78*, 191.
16. Harker, L. A.; Hanson, S. R.; Kelly, A. B. *Thromb. Haemost.* **1995**, *74*, 464.
17. Kaiser, B. *Drugs Future* **1998**, *23*, 423.
18. Sanderson, P. E. J. *Annu. Rep. Med. Chem.* **2001**, *36*, 79.
19. Rao, M. S.; Olson, A. J. *Proteins* **1999**, *34*, 173.
20. Shaw, K. J.; Guilford, W. J.; Dallas, J. L.; Koovakkaat, S. K.; McCarrick, M. A.; Liang, A.; Light, D. R.; Morrissey, M. M. *J. Med. Chem.* **1998**, *41*, 3551.
21. Guilford, W. J.; Shaw, K. J.; Dallas, J. L.; Koovakkat, S.; Lee, W.; Liang, A.; Light, D. R.; McCarrick, M. A.; Whitlow, M.; Ye, B.; Morrissey, M. M. *J. Med. Chem.* **1999**, *42*, 5415.
22. Sturzebecher, J.; Sturzebecher, U.; Vieweg, H.; Wagner, G.; Hauptmann, J.; Markwardt, F. *Thromb. Res.* **1989**, *54*, 245.
23. Renatus, M.; Bode, W.; Huber, R.; Sturzebecher, J.; Prasa, D.; Fischer, S.; Kohnert, U.; Stubbs, M. T. *J. Biol. Chem.* **1997**, *272*, 21713.
24. Padmanabhan, K.; Padmanabhan, K. P.; Tulinsky, A.; Park, C. H.; Bode, W.; Huber, R.; Blankenship, D. T.; Cardin, A. D.; Kisiel, W. *J. Mol. Biol.* **1993**, *232*, 947.
25. Goodsell, D. S.; Olson, A. J. *Proteins* **1990**, *8*, 195.
26. Morris, G. M.; Goodsell, D. S.; Halliday, R. S.; Huey, R.; Hart, W. E.; Belew, R. K.; Olson, A. J. *J. Comput. Chem.* **1998**, *19*, 1639.
27. Brandstetter, H.; Kuhne, A.; Bode, W.; Huber, R.; von der, S. W.; Wirthensohn, K.; Engh, R. A. *J. Biol. Chem.* **1996**, *271*, 29988.
28. Lin, Z.; Johnson, M. E. *FEBS Lett.* **1995**, *370*, 1.
29. Benner, S. A. *Tetrahedron Lett.* **1981**, *22*, 1851.
30. Cherkasov, R. A.; Kutyrev, G. A.; Pudovik, A. N. *Tetrahedron* **1985**, *41*, 2567.
31. Pedersen, B. S.; Lawesson, S. O. *Tetrahedron* **1979**, *35*, 2433.
32. Dann, O.; Char, H.; Griessmeier, H. *Liebigs Ann. Chem.* **1982**, 1836.
33. Pinner, A.; Klein, F. *Chem. Ber.* **1877**, *10*, 1889.
34. Pinner, A.; Oppenheim: Berlin, 1892.
35. Liberman, A. L.; Vasina, T. V. *Zh. Org. Khim.* **1967**, *3*, 690.
36. Borgen, G.; Dale, J. *Acta Chem. Scand.* **1972**, *26*, 952.
37. Ito, Y.; Fuji, S.; Nakatsuka, M.; Kawamoto, F.; Saegusa, T. *Org. Synth.* 1976, *Collective Volume VI*, 327–333.
38. Sugimura, T.; Futagawa, T.; Tai, A. *Chem. Lett.* **1990**, 2291.
39. Lineweaver, H.; Burk, D. *J. Am. Chem. Soc.* **1934**, *56*, 658.
40. Dixon, M. *Biochem. J.* **1953**, *55*, 170.
41. Dowd, P.; Zhang, W.; Geib, S. J. *Tetrahedron* **1995**, *51*, 3435.
42. Batey, R. A.; Harling, J. D.; Motherwell, W. B. *Tetrahedron* **1996**, *52*, 11421.
43. Kharasch, M. S.; Tawney, P. O. *J. Am. Chem. Soc.* **1941**, *63*, 2308.
44. Ouari, O.; Chalier, F.; Bonaly, R.; Pucci, B.; Tordo, P. *J. Chem. Soc., Perkin Trans. 2* **1998**, 2299.
45. Robson, C.; Meek, M. A.; Grunwaldt, J. D.; Lambert, P. A.; Queener, S. F.; Schmidt, D.; Griffin, R. J. *J. Med. Chem.* **1997**, *40*, 3040.
46. Harding, K. E.; Ligon, R. C.; Tseng, C. Y.; Wu, T. C. *J. Org. Chem.* **1973**, *38*, 3478.
47. House, H. O.; Kinloch, E. F. *J. Org. Chem.* **1974**, *39*, 1173.
48. Sheldon, J. C.; Taylor, M. S.; Bowie, J. H.; Dua, S.; Chia, C. S. B.; Eichinger, P. C. H. *J. Chem. Soc., Perkin Trans. 2* **1999**, 333.
49. Hall, S. R. d. B.D.J.; Olthof-Hazekamp, R. *Xtal3.7 System*; University of Western Australia: Crawley, Western Australia, 2000.
50. Sheldrick, G. M. *Acta Crystallogr., Sect. A: Found. Crystallogr.* **1990**, *A46*, 467.
51. Bode, W.; Turk, D.; Karshikov, A. *Protein Sci.* **1992**, *1*, 426.